Available online at www.sciencedirect.com
SCIENCE DIRECT
Journal of Power Sources 158 (2006) 274–286
JOURNAL OF POWER SOURCES
www.elsevier.com/locate/jpowsour

Modeling and simulation of a PEM fuel cell stack considering temperature effects

Yuyao Shan *, Song-Yul Choe

Department of Mechanical Engineering, Auburn University, AL 36849, USA

Received 9 August 2005; accepted 4 September 2005
Available online 2 February 2006

Abstract

Management of the water and heat ejected as byproducts in an operating PEM fuel cell stack are crucial factors in their optimal design and safe operations. Models currently available for a PEM fuel cell are based on either empirical or 3-D computational fluid dynamics (CFD). Both models do not fully meet the need to represent physical behavior of a stack because of either their simplicity or complexity. We propose a highly dynamic PEM fuel cell stack model, taking into account the most influential property of temperature affecting performance and dynamics. Simulations have been conducted to analyze start-up behaviors and the performance of the stack in conjunction with the cells. Our analyses demonstrate static and dynamic behaviors of a stack. Major results presented are as follows: (1) operating dependent temperature gradient across through-plane direction of the fuel cell stack, (2) endplate effects on the temperature profile during start-up process, (3) temperature profile influences on the output voltage of individual cells and the stack, (4) temperature influence on the water content in membranes of different cells, and (5) cathode inlet relative humidity influence on the temperature profile of the stack.

Keywords: PEMFC; Stack; Start-up; Dynamics; Temperature

1. Introduction

The PEM fuel cell is a potential candidate for use as an alternative power source in future vehicle and power conditioning applications. The electric power, as a load, continuously varies with a function of time in the systems. Accordingly, the flow rates of fuels and reactants should be properly supplied to meet the dynamics of load requirement. Hence, temperature and humidity for the stack should be precisely maintained to secure an efficient, safe, and durable operation of the PEM fuel cell system.

The complexity of these interrelated physical phenomena impedes design and system engineers from optimizing design parameters and criterion that lead to high costs and engineering time. Utilization of computer models have been proven to be the most effective tool requiring a comprehensive physical model reflecting real behaviors of the fuel cell stack.

Currently, models can be classified into two groups: a simple composition of passive electric circuit representing the double layer effects with a voltage source using *I–V* empirical curve [1,2], and a relatively precise cell model based on CFD [3–5] whose behavior is governed by equations describing chemical reactions, fluid and thermodynamic, and electric properties. These CFD models take enormous computational time necessary for a calculation of grid points and constrain the wide use of the models. Moreover, associated parameters and variables required for the models are hard to characterize and measure because of the thinness of layers during operations. Thus, these models are mostly applied to investigate parts of complex domains such as flow fields of a single cell and predict the cell performance with a constant temperature. A possible loophole has been proposed by other authors with lumped models emphasizing dynamic behavior of the stack. For example, Amphlett et al. [6] developed a first dynamic model with empirical thermal values, and Gurski et al. [7] expanded it to consider reactant flow and coolant control. Further improvement was made by Muller and Stefanopoulou [8], who calculated the temperature variation of a stack. However, the simulation results do not incorporate either the dynamic

* Corresponding author. Tel.: 1 334 844 3381; fax: 1 334 844 3307.
E-mail address: shanyuy@auburn.edu (Y. Shan).

0378-7753/$ – see front matter © 2005 Elsevier B.V. All rights reserved.
doi:10.1016/j.jpowsour.2005.09.053

Nomenclature

A	area (m^2)
C	mass concentration ($kg\,m^{-3}$)
C_p	specific heat
F	Faraday number
I	current density ($A\,m^{-2}$)
l	thickness (M)
m	mass (kg)
M	mole mass ($kg\,mol^{-1}$)
P	pressure (partial pressure) (Pa)
R_{ele}	electrical resistance (Ω)
S	entropy ($J\,mol^{-1}\,K^{-1}$)
T	temperature (K)

Superscripts and subscripts

cv	control volume
g	gas
i, j	index
l	liquid
an	anode
ca	cathode
sat	saturation
sou	source

or transient aspects of the fuel cell system in operating environments.

These drawbacks have been significantly complemented by using simplified thermodynamic models to analyze the performance of the stack, by Sundaresan and Moore [9]. His model based on layers is used to analyze the start-up behavior from a sub-freezing temperature. However, the model does not fully consider several factors: (1) flow of species at the inlet must be the same as that at the outlet. Thus, no fluid dynamics are considered in the model. (2) Heat source terms in both the catalysts are empirically calculated with values suggested by Wohr and Peinecke's modeling [10,11]. Accordingly, the anode source term is presumed as a relatively large value that should be referred to be around zero [12]. As a result, the model does not show asymmetric phenomena of performance across the stack.

Wetton et al. [13] proposed an explicit thermal model with the coolant channel coupled with a 1-D cell model [14], which shows an outstanding temperature gradient of the stack, but with no dynamics at all.

In fact, dehydration of membranes dynamically varies with temperature, which strongly influences overall performance of cells and finally the resulting stack. Consequently, a high dynamic model for a stack based on layers of a single cell [15] has been developed by reflecting the dynamics under different operating conditions for pressure, humidity, reactants and temperature. Temperature profiles in a stack with associated effects on the stack performance show the high dependency in not only static but also dynamic behavior.

2. PEMFC stack modeling

2.1. Assumptions and domain

Assumptions made are as follows:

1. reactants as ideal gases;
2. no pressure gradient between the anodic and cathodic side, which results in no convection, but only diffusion for gas transport;
3. identical inlet conditions of each cell for both the cathode and anode as well as coolant channel;
4. no gas pressure drop along the gas channel;
5. linear temperature gradient, linear across the layers in the stack;
6. constant thermal conductivity of the materials in a fuel cell;
7. no contact resistance;
8. negligible anodic over-potential;
9. no current density gradient across the cathode catalyst layer, which implies a complete reaction of reactants at the cathode catalyst layer surface.
10. the anodic stoichiometrical coefficient is 1, which indicates a complete reaction of the fuel filled in the fuel cell stack.

Based on these assumptions, a layered based model for a 10-cells stack is developed. The schematic configuration of the simulation domain for the stack is shown in Fig. 1, where the cathode sides of the cells are located on the left-hand side, while the anodic on the right-hand side.

2.2. Single cell

2.2.1. Governing equations

A model for a single cell has been developed with compositions of individual layers and the performance detailed analyzed [15]. Table 1 summarizes the sub-models the governing the equations describing phenomenon for a single cell [15].

2.2.2. Thermal model

The fuel cell is sandwiched between two bipolar plates. The individual layer of a single cell and a bipolar plate is regarded as a control volume, whose thermal-physical properties are isotropic and constant. Then, according to the energy conservation equation, the total energy changes in a control volume are equal to the sum of the energy exchange at boundaries and internal

Table 1
Equation system of the single cell model

Sub-models	Phenomenon	Mathematical equation
Electrochemical model	Chemical reaction	Butler–Volmer
Layered thermal model	Temperature variation	Energy conservation
Membrane water balance	Water transport	1-D mass conservation
Catalyst layer proton model	Proton concentration variation	Empirical
GDL O_2 diffusion model	Multi-component diffusion	1-D Stefan–Maxwell
Gas channel mass balance		0-D mass conservation

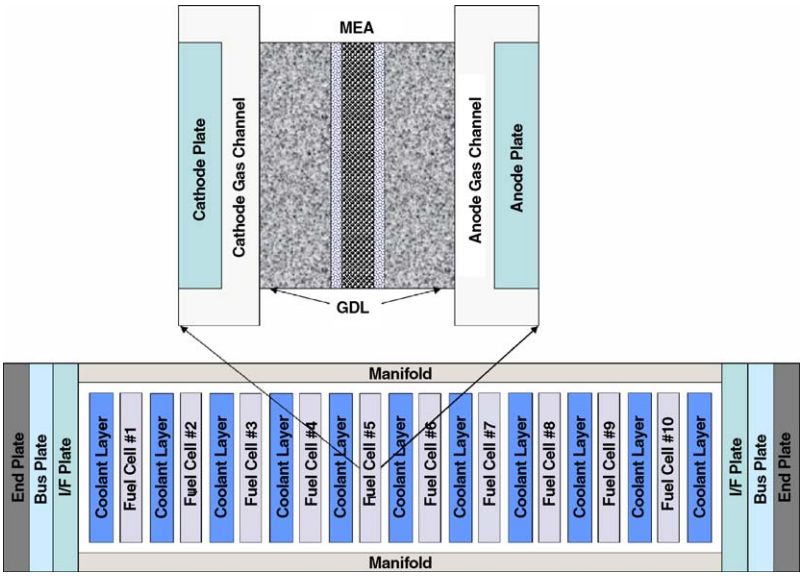

Fig. 1. Stack schematic configuration.

energy resources. The energy exchanges at boundaries occur by three factors: (1) mass flow into each volume; (2) conduction heat transfer through the cell; (3) convection heat transfer between the reactants and bipolar plates with the coolant. Thus, the thermal–dynamic behavior can be described by using the following energy conservation equation:

$$\sum_i C_p C_{i,\mathrm{mass}} A_{\mathrm{cell}} l_{\mathrm{cv}} \frac{\mathrm{d}T_{\mathrm{cv}}}{\mathrm{d}t} = \underbrace{\sum \dot{m}_{\mathrm{in}} A_{\mathrm{cell}} C_p (T_{\mathrm{in}} - T_{\mathrm{cv}})}_{\text{Mass flow in}} + \underbrace{\dot{Q}_{\mathrm{Conv}} A_{\mathrm{cell}}}_{\text{Convection heat transfer}} + \underbrace{\dot{Q}_{\mathrm{Cond}} A_{\mathrm{cell}}}_{\text{Conduction heat transfer}} + \underbrace{\dot{Q}_{\mathrm{sou}}}_{\text{Sources}} \quad (1)$$

Hence, the internal energy source is mainly composed of the entropy loss and the chemical energy required for oxygen and protons to overcome the barrier of the over-potentials in both catalyst layers (Eq. (2)). In addition, other heat sources are associated with ohmic losses by a transport of electrons and protons in a cell:

$$\dot{Q}_{\mathrm{sou}} = i A_{\mathrm{cell}} \left(-\frac{T \Delta S}{4F} + \eta + i A_{\mathrm{cell}} R_{\mathrm{ele}} \right) \quad (2)$$

In fact, the change in entropy due to the electrochemical reaction (Eq. (3) and (8)) in both of the catalysts sides predominantly influences the energy sources term, which can be clarified by the calculations below.

The chemical reaction of the cathode catalysts can be described as,

$$O_{2(g)} + 2H^+_{(aq)} + 2e^- \rightleftharpoons H_2O_{(l/g)} \quad (3)$$

Therefore, the entropy change of the cathode reaction is equal to the sum of that in water, oxygen and electron. The phase of water produced can be either vapor or liquid which makes a difference in the entropy change of the reaction. The value of the entropy change indirectly measured by Ref. [16] amounts to 52 J mol^{-1} K^{-1}. However, this value is quite different from other authors [3,17,18]. Therefore, the energy generated in a catalyst layer for three cases are calculated and the values are compared for a better judgment.

The first case assumes water generated as vapor phase. Then, the cathode entropy change can be described as follows:

$$nF\frac{\partial E_o}{\partial T} = \Delta S_{\mathrm{ca}} = s[H_2O_{(g)}] - \frac{1}{2}s[O_{2(g)}] - 2s[e^-_{pt}] = 198 - \frac{1}{2} \times 205.03 - 2 \times 65.29 = -35.095\ \mathrm{J\,mol^{-1}\,K^{-1}} \quad (4)$$

The resulting energy by the entropy change is equal to:

$$Q = \Delta S_{\mathrm{ca}} T = -35.095T\ \mathrm{J\,mol^{-1}\,K^{-1}}$$

The second case assumes water as liquid phase. The corresponding entropy change of the reaction and the energy result in as follows:

$$nF\frac{\partial E_o}{\partial T} = \Delta S_{\mathrm{ca}} = s[H_2O_{(l)}] - \frac{1}{2}s[O_{2(g)}] - 2s\left[e^-_{pt}\right] = 69.91 - \frac{1}{2} \times 205.03 - 2 \times 65.29 = -163\ \mathrm{J\,mol^{-1}\,K^{-1}} \quad (5)$$

$$Q = \Delta S_{\mathrm{ca}} T = -163T\ \mathrm{J\,mol^{-1}\,K^{-1}} \quad (6)$$

The last case assumes that the water generated is immediately evaporated at the catalysts. The corresponding energy required for the evaporation can be expressed as a product of the latent heat and the rate of mass change from liquid phase to vapor:

$$Q = h_{fg}\dot{m}_{fg} \tag{7}$$

A comparison with the experimental value [16] indicates that most parts of water generated might be a state of vapor. Later in Section 3, simulations have been conducted for the first two cases.

In contrast, the anodic side is assumed to be a standard electrode, while the membrane is assumed to provide a water-like environment. Thus, the anodic entropy change becomes almost zero.

$$H_{2(g)} \rightleftharpoons 2H^{+}_{(aq)} + 2e^{-}_{(pt)} \tag{8}$$

2.3. Stack

The model for a stack consists of models for endplates assembly, multiple single cells and coolant channels as in a typically designed stack. The stack voltage and current are obtained by series and parallel connections of outputs of individual cells, while the thermal conditions for each of the cells and coolant channels, or between coolant channels and endplate assembly, are coupled by using the energy conservation equation (Eq. (1)).

3. Simulation results

All of the aforementioned models are coded with Matlab/Simulink and C. Simulations with different operating conditions have been conveyed to investigate the static and dynamic behavior of a single as well as a stack, which include the typical polarization curves at different working temperatures, a start-up behavior and transient responses of the stack on a current as a step load.

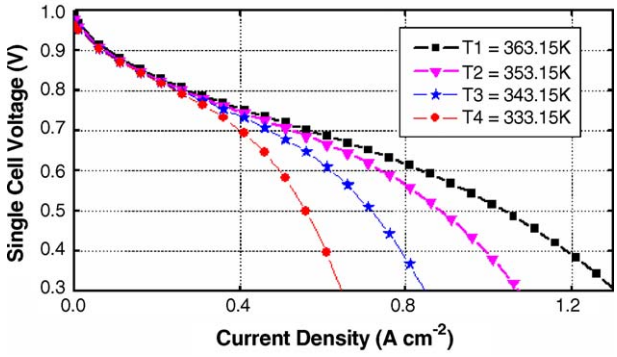

Fig. 2. *I–V* curve for different cell working temperature.

3.1. Parameters

The parameters used for models are summarized as follows (see Table 2).

3.2. Polarization curve

Fig. 2 shows the temperature dependent *I–V* characteristics from 333 to 363 K with a step of 10 K. As the temperature increases, the water removal is easier. The effects are considerably high at the range of the higher cell current, where more water is produced. This result is comparable with an analysis using CFD [19].

3.3. Dynamic behaviors

Currently, lack of experimental data on the water phase inside cells impedes any statement on how much of the enthalpy is generated by a water molecule, which includes decisive information on the state of water generated. Thus, the two cases of either the liquid or the vapor are selected and summarized as follows:

Case 1. If the RH of the cathode inlet is low and at the same time the stoichiometrical number on the cathode is high, water generated by the chemical reaction in the catalysts is immediately removed by the cathode outlet gas in the form of vapor.

Table 2
Geometrical parameters

	Thickness (m)	Heat conductivity ($W\,m^{-1}\,K^{-1}$)	Heat capacity ($J\,kg^{-1}\,K^{-1}$)	Density ($kg\,m^{-3}$)
GDL	0.0004	65	840	2000
Catalyst layer	0.000065	0.2	770	387
Membrane layer	0.000183	0.21	1100	1967
Gas channel	0.001	52	935	1400
Plate	0.001	52	935	1400
Coolant channel	0.001	30	935	1400

GDL porosity	0.5
GDL tortuosity	3.725
Bipolar plate contact area percentage	0.55
Membrane molecular mass ($kg\,mol^{-1}$)	1.1
Fuel cell area (m^2)	0.0367
Fuel cell active area (m^2)	0.03

Table 3
Operating condition of the stack

Gas inlet condition	P_{in}	φ_{in}	RH_{in}	$f_{O_2 \text{ or } CO}$
Cathode	141000	2.5	0.2	0.21
Anode	141000	1	0.001 or 0.5	0

This state can be regarded as a vapor phase, where no liquid is formed in the stack. One of possible operating conditions is listed in Table 3 with other parameters necessary for a simulation:

Case 2. If the RH at the anodic inlet is high and stoichiometrical number at the cathode is low, then water generated at the catalysts cannot be removed immediately in the form of vapor in the cathode outlet gas. Thus, assumptions can be made that water is mainly generated and removed in the liquid phase. These cases are listed in Table 4 with the second condition. The simulation parameters are listed below.

The start-up and transient behaviors are analyzed by using these conditions and the simulated results are discussed in the following sections.

The operating conditions for a start-up and transient response are described as follows:

- The start-up temperature for the cells is initially set to 298.15 K. A look-up table was created for the lowest membrane temperature among the 10 cells as an input and the current density as an output. The value of current density continuously follows the increase of the temperature in the membrane in order to quickly raise the temperature to 353.15 K that is assumed as a typical working temperature. In addition, a built-in controller regulates the temperature in the membrane to prevent dehydration. Whenever the temperature in different cells exceeds the desired working temperature, a coolant subsystem is turned on and off to extract the excessive heat produced in the stack.
- A load current with multiple steps is applied to the stack model and the transient responses analyzed.

3.3.1. Start-up

3.3.1.1. Case 1: vapor phase (low cathode inlet RH and fast water removal). Fig. 3 shows the current load, the transient behavior of the temperature for the membrane layer of different cells, as well as the stack temperature profile at the 50, 360 and 450 s during the start-up. In the given start-up condition (Table 4); it took more than 6 min for a membrane layer with the highest temperature to reach the desired working temperature (Fig. 3b).

Generally, the temperature of each layer rises during a start-up. Due to ohmic losses by the membrane resistances and the heat released by the chemical reaction in the cathode catalysts, the membranes and cathode catalysts show the highest value among others. In contrast, the losses on the anodic side are negligible. Therefore, the high losses of cathodic catalysts and the corresponding heat generated leads to an asymmetrical temperature distribution throughout the cell [15,17,23].

Table 4
working condition of the stack

Gas inlet condition	P_{in}	φ_{in}	RH_{in}	$f_{O_2 \text{ or } CO}$
Cathode	141000	2.5	0.8	0.21
Anode	141000	1	0.001 or 0.5	0

In fact, the temperature of membranes rises to a reference temperature with the associated rising time strongly influenced by the location of a cell in the stack. As a result, the total heat capacity of an endplate assembly is much higher than the one of the layers in the cells. The heat generated in the end cells are quickly transferred to endplates and stored there rather than stored in the cell itself. The temperature of the membrane layers in the middle of the stack increases more rapidly than the end ones. For example, the 5th cell shows the highest temperature, while the 10th cell shows the lowest (Fig. 3b).

The profile of the stack temperature in Fig. 3c–e shows different dynamics with an asymmetric shape that differs from the one with symmetric shape [9] or smooth curve [20]. In addition, an unsteady and abrupt drop of temperature at the end cells is observed, caused by the difference between ambient and cell temperature. The large heat capacity of the bus plate and the small heat transfer coefficient of the endplate lead to a negligible heat transfer.

At the 50th second after the start-up (Fig. 3c), the nine cells show the temperature walls at MEA except the cell number 1. In fact, the cathode catalyst layer of the cell 1 is located near the endplate and possibly conducts a large amount of heat generated toward the endplates. Compared to the first cell, the heat generated at the cathode catalyst in the 10th cell is being kept by two more layers of the membrane and anodic catalysts. Thus, the temperature of the cathode catalysts layer in the first cell becomes lower than the one of the 10th cell.

At the 360th second (Fig. 3d), the membrane of the fifth cell shows the highest temperature at 80 °C, while six cells still show a temperature wall with an asymmetric distribution. The temperature wall is generated in the 10th cell before blocking the conduction of the heat generated by the rest of the cells. The transfer of heat occurs through the left side of cells. As a result, the temperature of the left end plate assembly rises more than the one of the right end plate assembly. Subsequently, the temperature walls of cells located at the right-hand side of the stack disappear. Then, the temperature of the cell rises gradually, while the first cell does continuously. Finally, the temperature of the cathode catalysts layer in the 10th cell becomes lower than the one of the first cell.

At the 450th second, the numbers of temperature walls increase again. As the temperature at the end plate assembly increases, the gradient of the cells and the end plates becomes lower and thus the heat conduction from the cells decrease. As a result, the heat generated accumulates in the end cells, while the heat in the inner cells causes a temperature rise in the coolant that offsets the end cells with a temperature rise. Finally, the temperature of the stack becomes more uniform. The middle cells reach a steady state, while the temperature dynamics of the end cells have not completed yet.

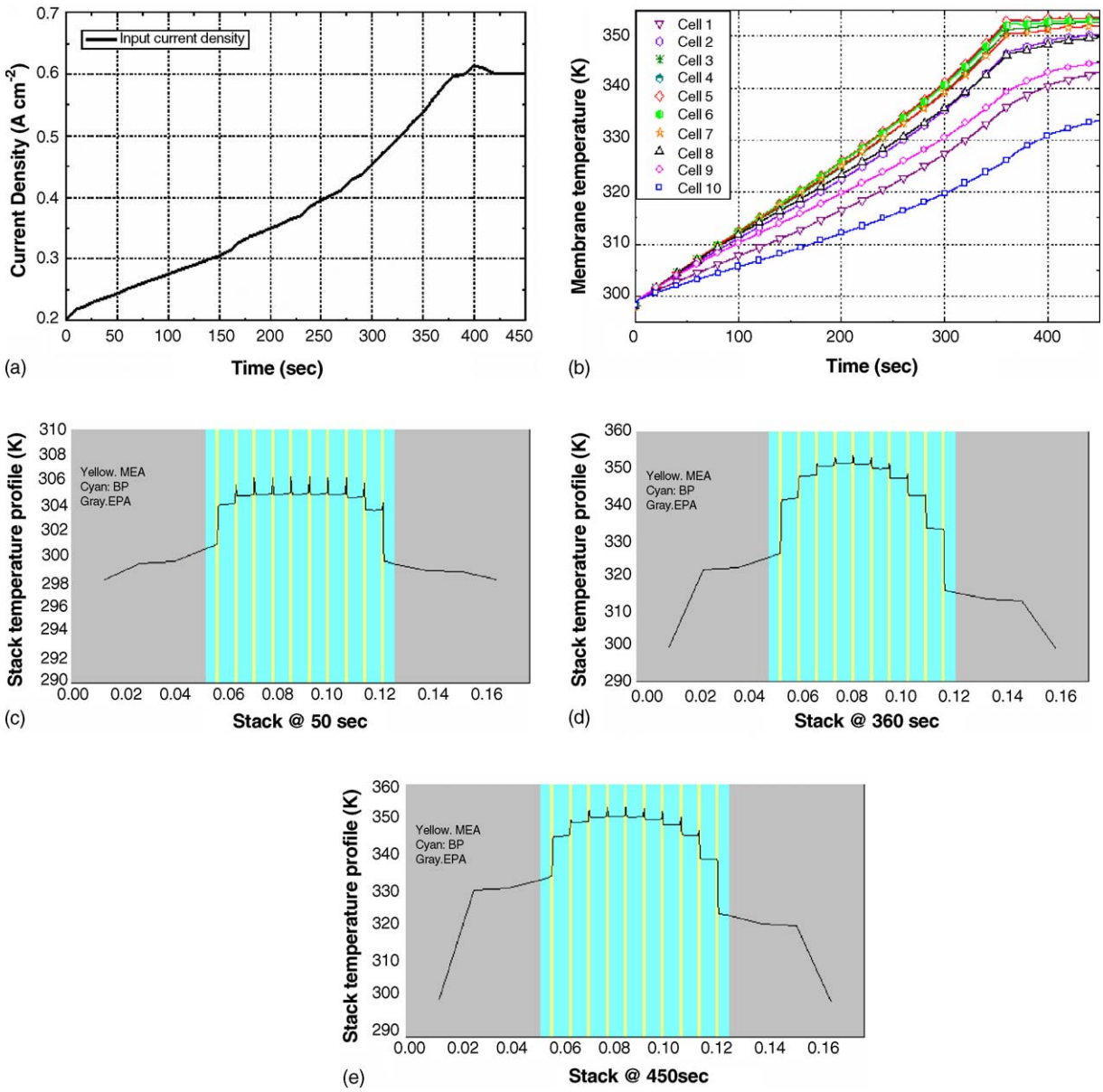

Fig. 3. (a) Current input for the start-up. (b) Dynamic membrane temperature of the 10 cells. (c) Stack temperature distribution at the 50 s. (d) Stack temperature distribution at the 360 s. (e) Stack temperature distribution at the 450 s.

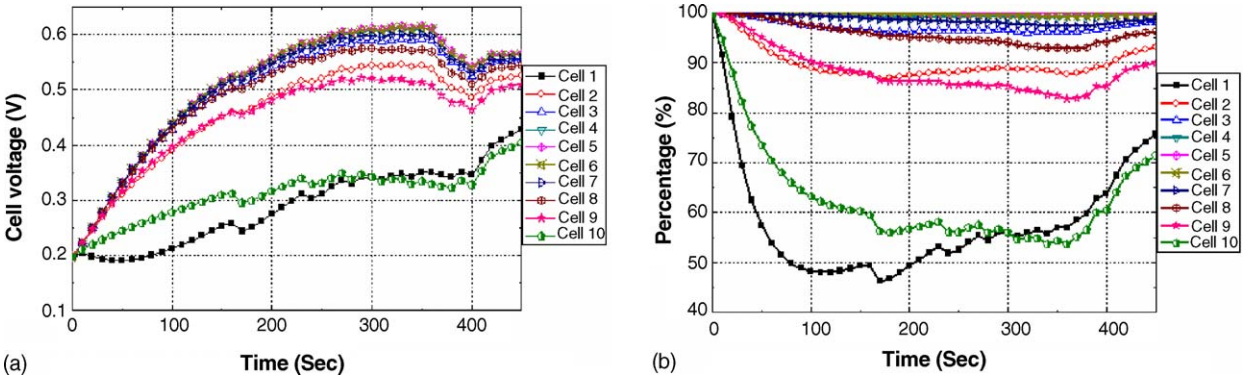

Fig. 4. (a) Dynamic voltage output of the 10 cells. (b) Voltage output percentage of the 10 cells.

Fig. 4 shows a dynamic behavior of the output voltage of the individual cell and output voltage referred to the fifth cell voltage that shows the highest value.

Generally, the cells located in the inner side of a stack show low losses of over-potentials because of the high temperature. The middle cells illustrate a higher output voltage than those of the end cells.

The behavior of the two end cells is particularly different from the rest of the cells (Fig. 4a). The voltage of all the cells tends to follow the increase of temperature but those of end cells show a decrease. In fact, the lower temperature at the end cells slows down the removal of water continuously generated, which blocks the influx of the reactants toward the catalysts through the GDL. Likewise, water generated in the catalyst is hard to remove, which causes a high over-potential. This simulation result is comparable to the experimental results [21].

The output voltage of the cells is shown in Fig. 4b. The voltage increases until 300 s and remains almost constant affected mainly by dehydrated membranes and the associated low proton conductivities. On the other hand, the 10th cell shows less loss in the over-potential than the first cell until 300 s, because the temperature of the cathode catalyst at the first cell becomes larger than the one at the 10th cell. As soon as the coolants start controlling temperature around 350 s, the output voltage of cells except two end cells starts decreasing until the current reaches around 0.6 A cm^{-2}. The operating condition of the anodic inlet RH is intentionally set to 0.6 from 0.001 in order to study the effects of the humidity on the membranes. As a result, the voltage of the cells starts increasing because of the increased membrane proton conductivity. The recovery speed of membrane conductivity of the individual cell becomes dependent on the cell location in the stack, whose physical reasons are described in detail in the following section.

Fig. 4b shows percentage rates of the cell voltages. The voltage of the end cells amounts to half of the voltage produced by the central cells. The derivation of the central cells varies at a rate of around 20%, which also worsens overall performance of the stack.

The proton conductivity of membrane currently available strongly depends upon water content. Therefore, an analysis is performed to study the effect of the anodic RH and cell location on membranes. The inlet RH has been drastically changed from 0.001 to 0.6 at the 380 s. Fig. 5 shows simulated results of the water uptake of membrane layers in the 10 cells during the start-up.

At the low anode inlet gas humidification, water present in the membrane is only influenced by water generated in the catalysts. Thus, the water uptake continuously decreases and corresponding proton conductivity gets lower.

At an application of a high humidification, the water uptake in the membranes of all the cells increases. Particularly, the cells at the right-hand side show a higher rate of water uptake than its counterpart in the stack. The differences in temperature between the cathodic electrodes of cells at the left-hand side of the stack and at the right-hand side leads to different saturating pressures (Eq. (9)), although the amount of water generated is the same at the load current. The lower the temperature of the cathode gas, the lower the saturation pressure. Thus, the outlet gas carries less water vapor out of cells, and consequently, the water concentration in the membrane becomes higher.

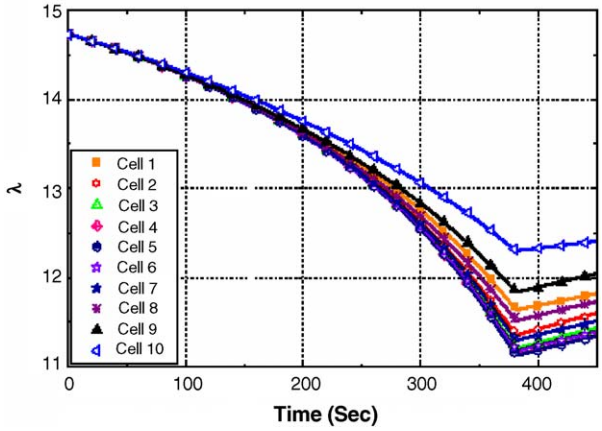

Fig. 5. Dynamic behavior of membrane water uptake for a stack.

$$P_{\text{sat}} = \begin{cases} 6.853\text{e}-7T^4 - 7.432\text{e}-4T^3 + 0.304T^2 - 55.613T + 3831.8 & \text{if } (T < 333.15\,\text{K}) \\ 6.853\text{e}-7T^4 - 7.432\text{e}-4T^3 + 0.304T^2 - 55.613T + 3831.8 & \text{if } (333.15\,\text{K} \le T < 433.15\,\text{K}) \end{cases} \quad (9)$$

A comparison of water uptake shows a large difference affected by the temperature distribution in the stack. For example, the central cells become quickly hydrated in comparison to the end cells. Under a fully consumed fuel, the anode gas gets saturated. Therefore, the electro-osmotic influence at the anodic boundary of each cell on their membranes becomes the same. However, the temperature distribution leads to much higher water concentration and diffusion coefficient in membrane layers at the central cells than the ones at the end cells.

If the influence of the liquid water is neglected, the diffusion of water from the anodic electrodes to membranes in the central cells becomes higher than the one in the end cells. Conversely, the humidity at the cathodic inlet is low and the temperature is high, so the gas is not saturated. Due to the temperature difference in the cells, the saturation pressure of end cells is lower than the one of the central cells (Eq. (9)) Consequently, water activity at the cathodic sides of the end cells is higher, which makes it easier to transport water out of membranes by electro-osmotic force at the cathode boundary. As a result, the recovery speed of water contents in the central cells is generally faster than the one in the end cells. However, the low water concentration in the cathode sides of the central cells accelerates water diffusion from membranes to cathodes, which again slows down the recovery speed.

3.3.1.2. Liquid phase (high cathode inlet RH and slow water removal). Fig. 6 shows the current load, the transient behavior of

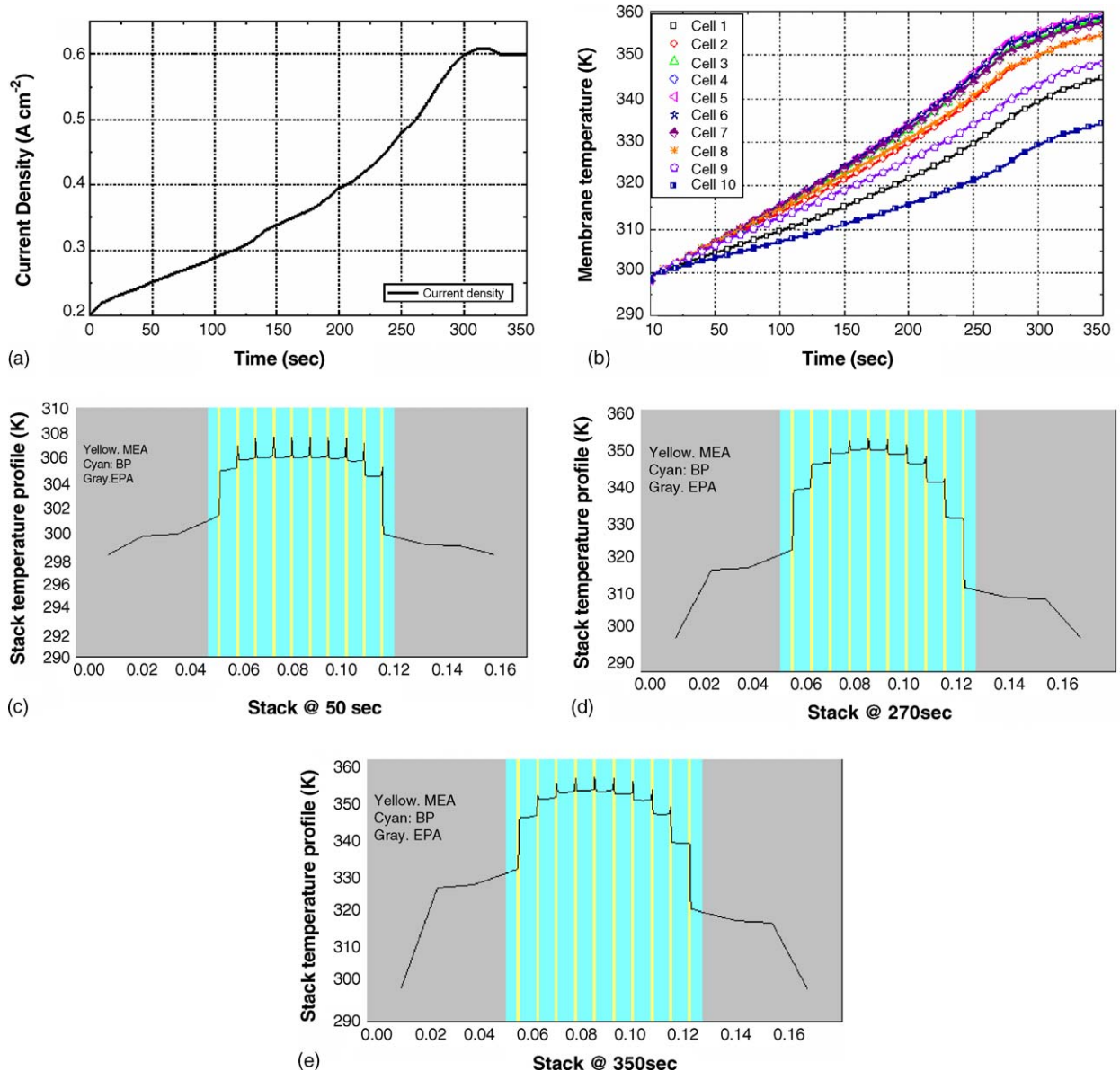

Fig. 6. (a) Current input for the start-up. (b) Dynamic membrane temperature of the 10 cells. (c) Stack temperature distribution at the 50 s. (d) Stack temperature distribution at the 270 s. (e) Stack temperature distribution at the 350 s.

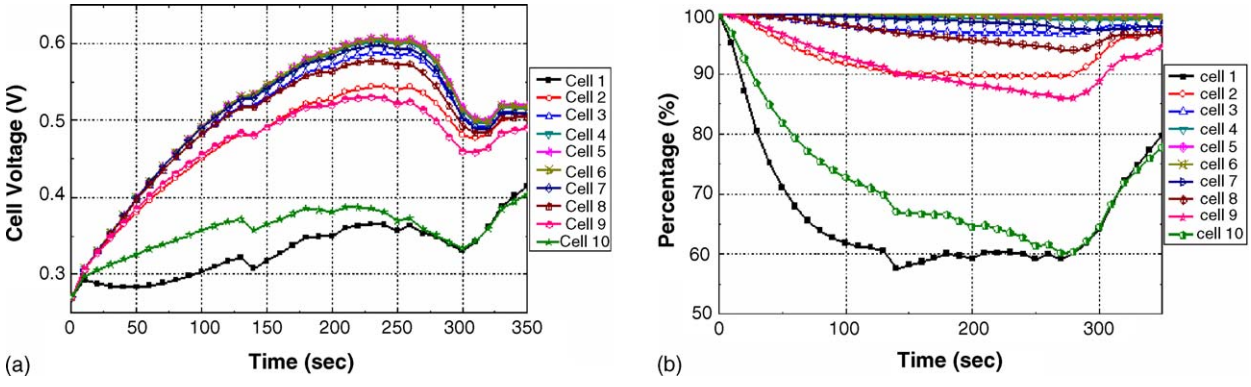

Fig. 7. (a) Dynamic voltage output of the 10 cells. (b) Voltage output percentage of the 10 cells.

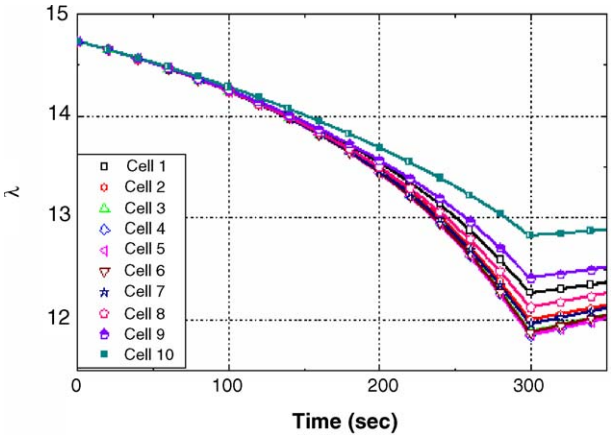

Fig. 8. Dynamic membrane water uptake of the 10 cells.

the temperature for the membrane layers of different cells as well as the stack temperature profile at the 50, 270 and 350 s. Even with the same lookup table of current and membrane temperature for the start-up, the speed of the start-up becomes quicker than the one in the first case. It takes about 4.5 min for the membrane layer with the highest temperature among others to reach the desired working temperature. In fact, the water generated in the cell is removed as liquid phase, so the latent heat necessary for getting water evaporated is stored in the stack. Fig. 6b shows the temperature waveforms of membranes. A comparison between Figs. 3b and 6b shows two differences: (1) temperature of membranes continuously rises, even if the coolant circuit turns on and (2) the gap between the membrane temperature of the 5th cell and the 10th cell is calculated by the time the coolant circuit turns on 75 s later. The difference in both gaps

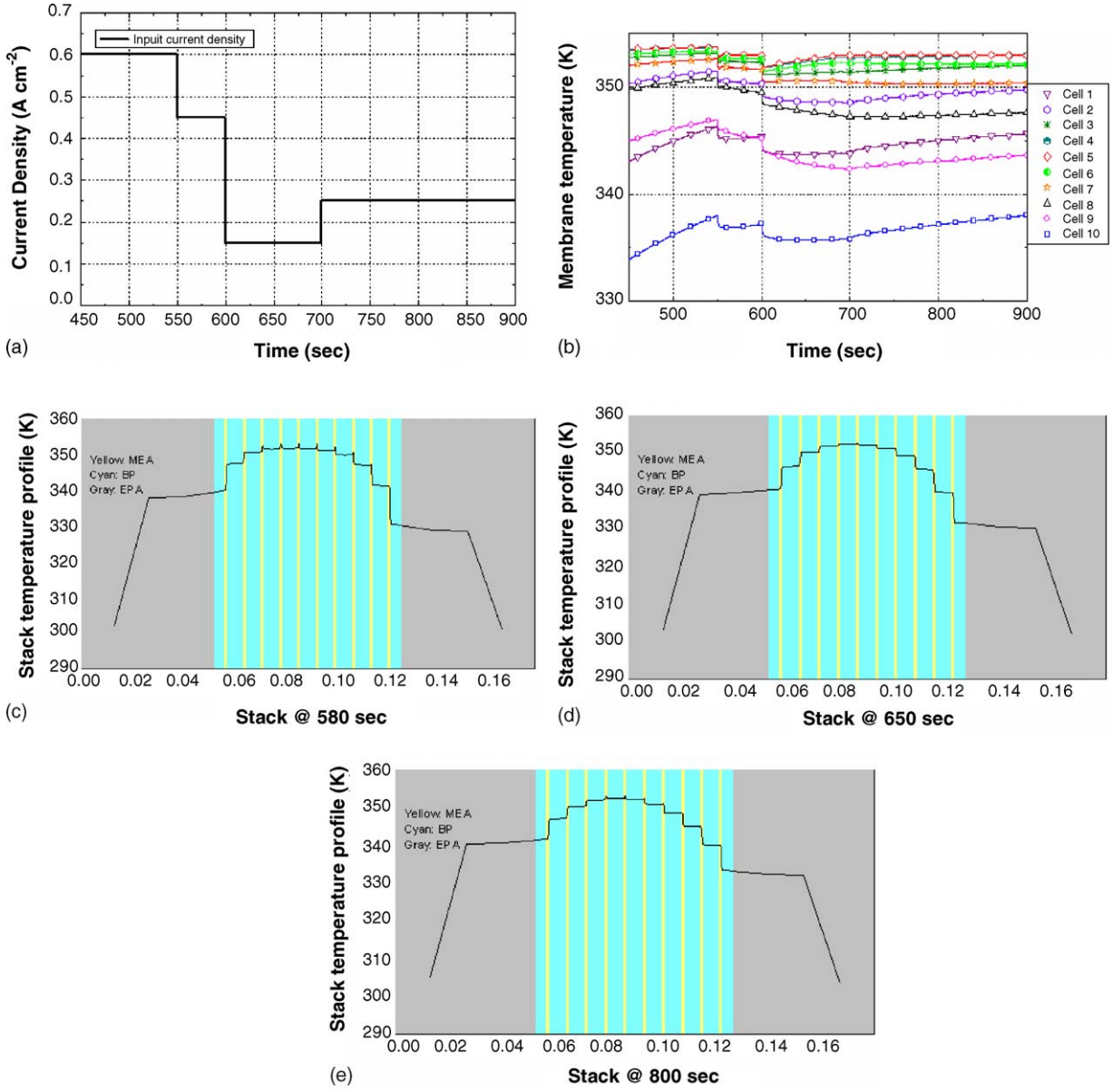

Fig. 9. (a) Step current input. (b) Dynamic membrane temperature of the 10 cells. (c) Stack temperature distribution at the 580 s. (d) Stack temperature distribution at the 650 s. (e) Stack temperature distribution at the 800 s.

has been decreased from 8 °C in the first case to 2 °C in this case.

Therefore, the low RH at cathode inlet in the first case enables the coolant to easily control the stack temperature at the start-up.

Fig. 6 d–f show the stack temperature profile at the 50, 270 and 350 s. A comparison with the first case shows relatively higher walls of temperature with increased numbers in the stack.

Fig. 7 shows the dynamic response of the output voltage of the 10 cells on the load current and the corresponding percentage rate. A comparison with the first case shows a low output voltage at about 0.6 A cm^{-2}, even though the temperature of the stack and membrane conductivity are higher than before. As a matter of fact, the liquid water generated at the catalysts layers blocks the influx of oxygen and finally leads to a starvation of oxygen.

Fig. 8 shows the water uptake in the membrane layer of the 10 cells at the start-up. The humidified cathode inlet gas slightly slows down dehydration of the membranes until the 300 s when the anode inlet gas starts to be humidified from 0.001 to 0.6. Then the water uptake of the membrane stops decreasing. A comparison with the results from the changed cathode and anode inlet gas RH shows that water transport at the boundary of membranes is dominated by the electro-osmotic drag force. Therefore, humidification on the cathode inlet gas is not sufficient to prevent dehydration, which requires additional humidification of the gas at the anodic inlet.

3.3.2. Transient response

3.3.2.1. Case 1: vapor phase (low cathode inlet RH and fast water removal). Fig. 9 shows the load current and the simulated results for the temperature of the membrane layers and the stack at the 580, 650 and 800 s.

When the current drops with 0.15 and 0.3 A cm^{-2}, the temperature of all membranes drops by 1° and 1.5°, respectively (Fig. 9b). Primarily, the heat associated with the current density is responsible for the rise or drop in temperature. Therefore, the recovery behavior and final value is strongly influenced by the amount of heat dependent upon the amplitude of current density. For example, a step with a high current density (0.45 A cm^{-2}) causes an immediate rise in temperature, while a low current density (0.15 A cm^{-2}) takes 100 s for the central membrane to reach a desired working temperature of 353.15 K.

The simulation shows that the temperature rise of the end cells at the high current density is faster than the one at the low current. Besides, the heat depends upon the current density because the coolant controlling for a working temperature carries over the heat from the central cells and offsets the temperature of the end cells. Similarly, the transfer of the heat to the end cells gets smaller. When the amplitude of the current is small, the corresponding heat generated in the central cell becomes smaller. Those effects are illustrated in Figs. 9d–f.

Fig. 10 shows the dynamic response of the cell output voltage and membrane water uptake of the 10 cells at the same load

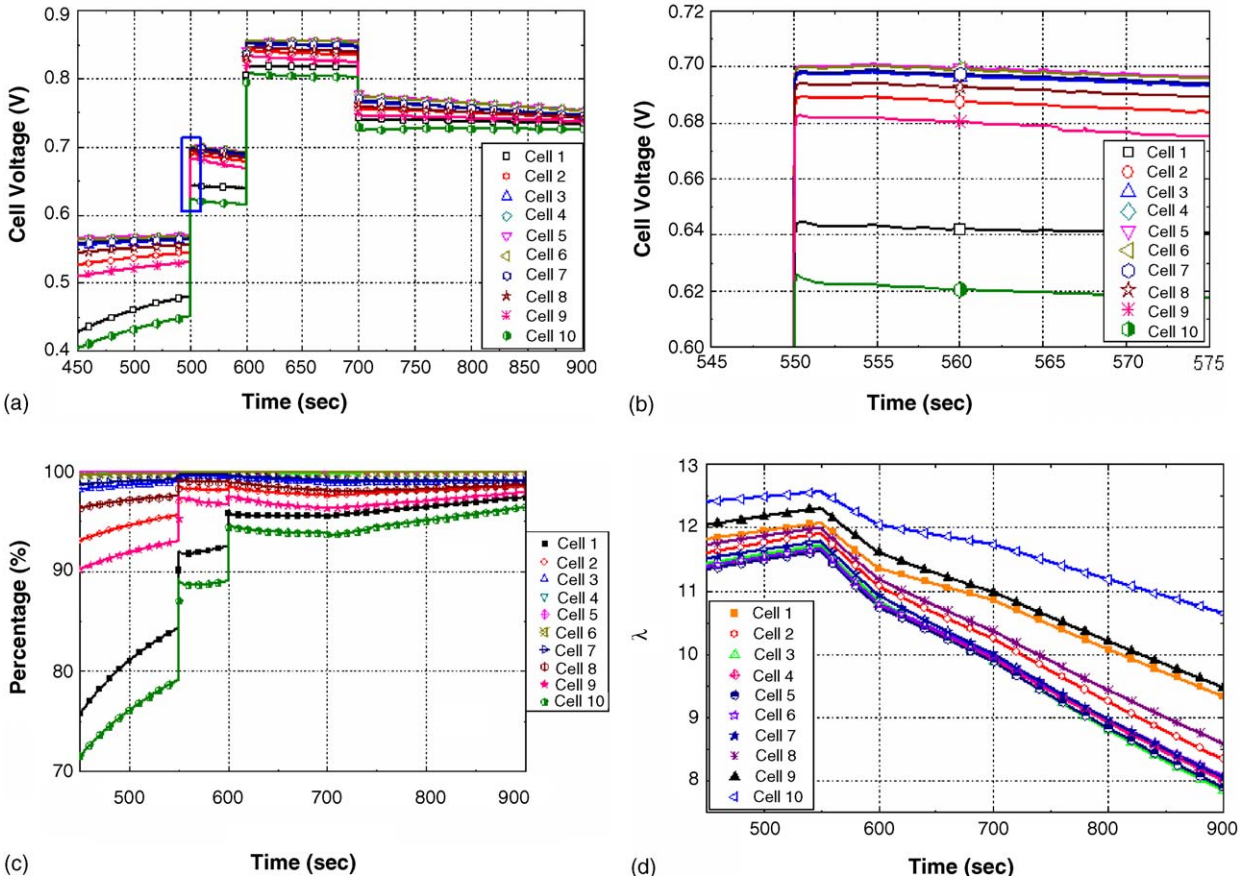

Fig. 10. (a and b) Dynamic voltage output of the 10 cells. (c) Voltage output percentage of the 10 cells. (d) Dynamic membrane water uptake of the 10 cells.

current. The overshoot of voltage is caused by several physical factors: (1) proton concentration at the cathode catalysts [16], (2) oxygen concentration at the catalyst [22], and (3) variation of the cell working temperature. Temperature influences the water saturation pressure (Eq. (9)) and the effective areas of cathode catalysts as well as oxygen concentration. More details are discussed in Section 3.3.2.2.

Fig. 10b and c shows responses of water uptake on the load current. The operating condition for the RH at the anode inlet is set to 0.001 from 0.6 at about 550 s when the current density is lower than 0.6 A cm^{-2}. The dependency of the membrane water uptake on the temperature is identical with the previous analyses.

3.3.2.2. Case 2: liquid phase (high cathode inlet RH and slow water removal). The step load current has been applied to study the effects of liquid water removal on the dynamics (Fig. 11a). Fig. 11b–f show the dynamic temperature behavior of the membrane layers and the stack temperature profile at the 400, 550 and 800 s. A comparison with the first case of operating condition shows a high temperature drop in the stack. It is caused by the large amount of heat generated in the catalysts when water is generated and removed as liquid. Consequently, the temperature cannot be controlled with the set coolant flow rate until the current density is decreased. At round 900 s, the temperature difference between the membrane of the central cell and two end cell amounts to about 5 and 13 °C, respectively, less than the previously calculated values of 5.5 and 15 °C even at the same amplitude of the current load.

Generally, the amplitude of the peak temperature at both high and low current density is higher than the first case and

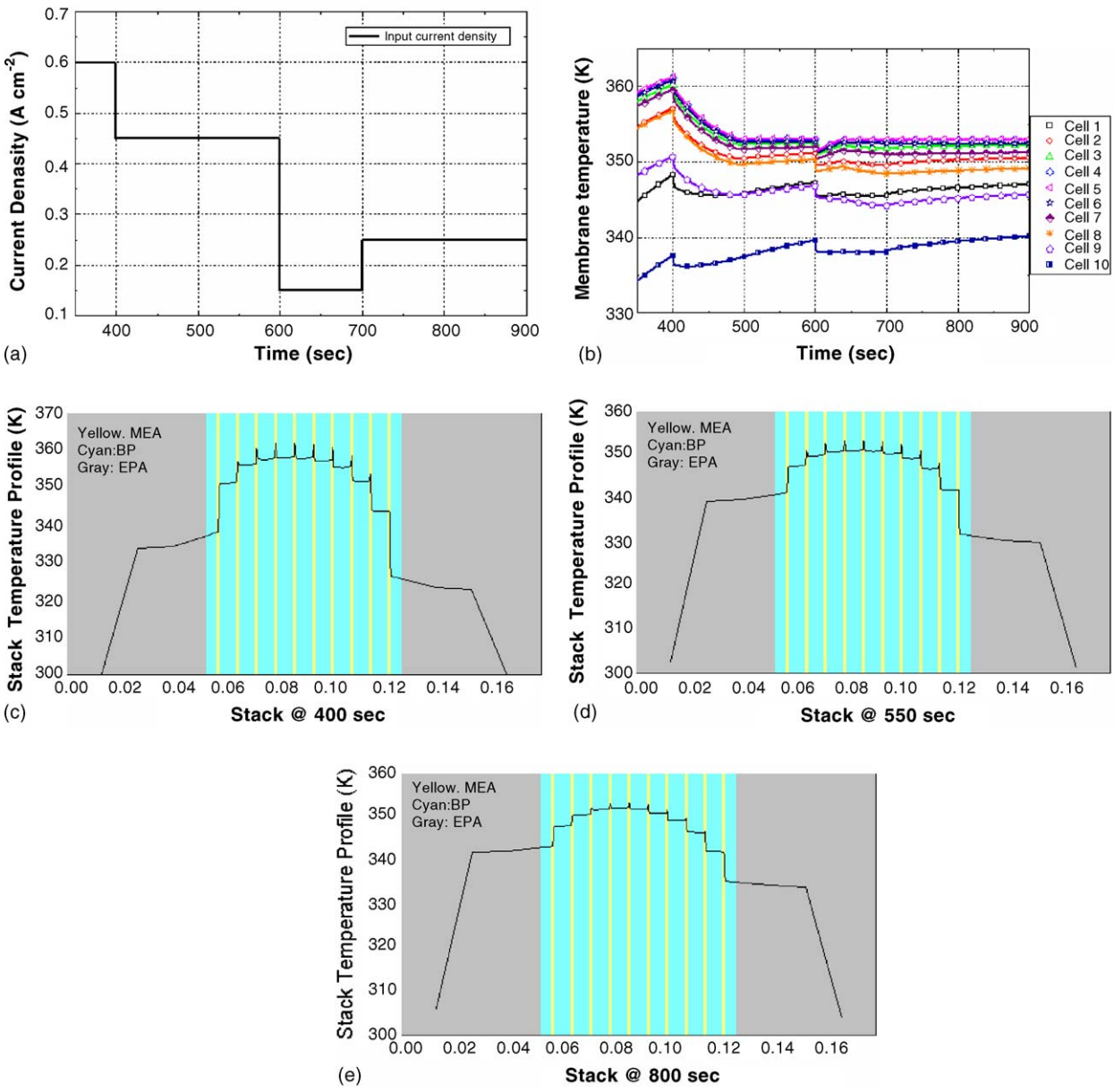

Fig. 11. (a) Step current input. (b) Dynamic membrane temperature of the 10 cells. (c) Stack temperature distribution at the 400 s. (d) Stack temperature distribution at the 550 s. (e) Stack temperature distribution at the 800 s.

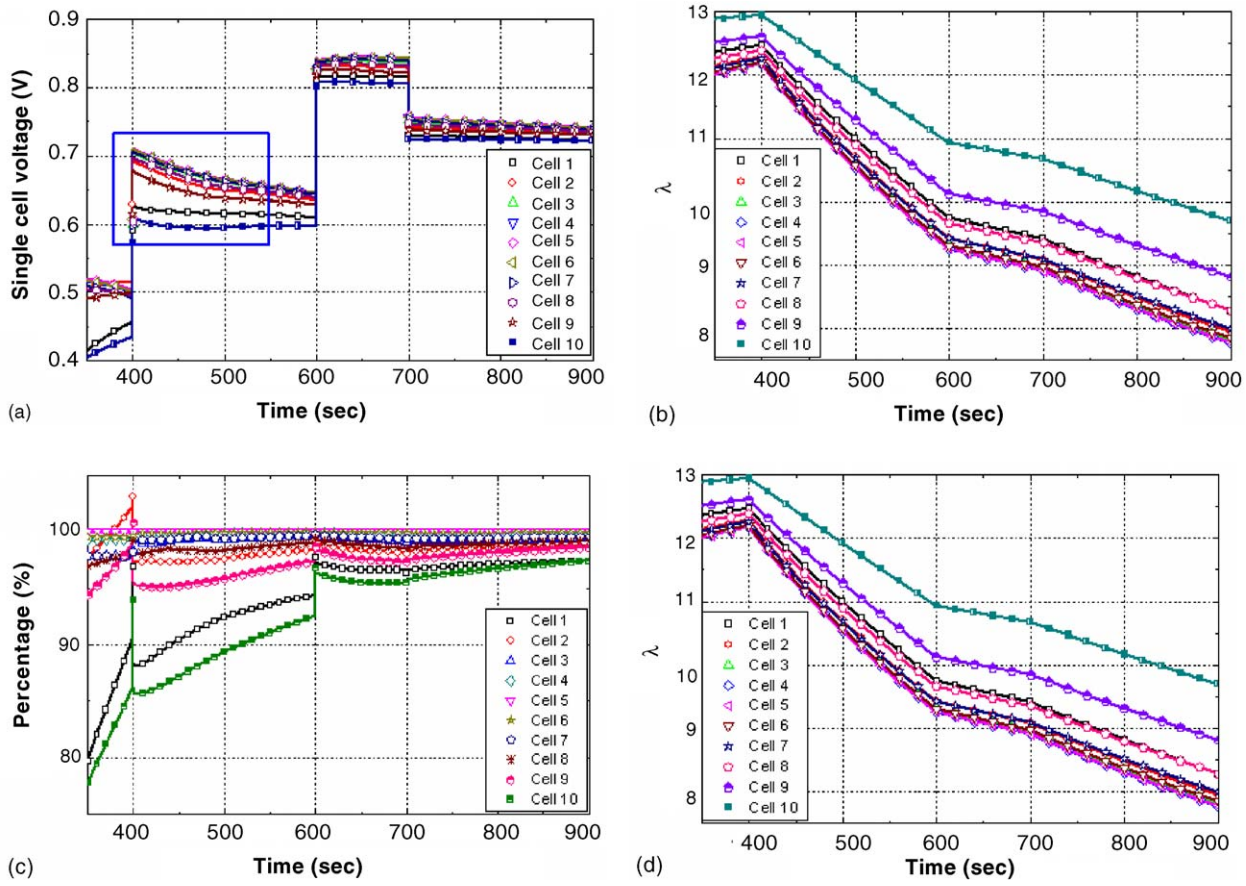

Fig. 12. (a and b) Dynamic voltage output of the 10 cells. (c) Voltage output percentage of the 10 cells. (d) Dynamic membrane water uptake of the 10 cells.

the numbers of temperature walls at MEA is more than before (Fig. 11d–f).

Fig. 12 shows the same dynamic responses of output voltage of all the cells. The amplitude of the overshoot of the output cell voltage is much larger than the first case according to Fig. 7a, which is strongly dependent on the temperature. An analysis shows that a sudden temperature drop with a high current causes high amplitude of the overshoot. Conversely, at the low current step, the heat generated can be more effectively extracted by the same condition of the coolant circuit, so the influence of temperature on the voltage overshoot becomes less.

In addition, the waveform of voltage of the 10 cells does not have the same tendency but fluctuates with distortions at special operating conditions. For example, the output voltage of the second cell at an instant can be higher than the fifth cell expected with the highest voltage. The open circuit voltage (OCV) is a function of the temperature whose derivative shows a negative value. Therefore, OCV decreases when the temperature rises. Consequently, the second OCV is higher than the fifth. In addition, the high temperature causes more water to be stored as vapor at the electrodes. Particularly, the second cell has lower temperature than the one in the fifth, which leads to a less water vapor. The concentration of oxygen becomes larger and the associated over-potential does smaller.

On the other hand, temperature increase accelerates dehydration of the membranes (Fig. 12c) that decreases the membrane proton conductivity. Therefore, corresponding proton conductivity of the second cell is higher than the fifth cell. Although the liquid water in the fifth cell is less than the one in the second, the overall cell performance of the second cell is better because of the three reasons aforementioned.

4. Conclusion

This paper presents a model for the PEM fuel cell stack based on single cells with layers. Simulation is conveyed to analyze the effects of temperature on static and dynamic characteristics of cells and finally the stack. Two operating conditions are considered to investigate behaviors of the stack at a start-up and a step load. The results show asymmetrical temperature distributions through the stack, varying dynamically with operating conditions and applied loads. The analyses suggest a new consideration for design and operating criteria to improve the performance of cells and optimize components of the power system. In particular, proper thermal management is required to prevent dehydration of membranes and secure longevity of the cells. Likewise, optimal operations of the stack can be derived by this simulation and associated new control strategies can be developed. Major findings are summarized as follows:

- Temperature distribution through the cells is asymmetric because of the heat generated in the cathode sides are higher than in the anodic sides. This asymmetric effect coupled with the end plate finally leads to an asymmetrical temperature

profile in the stack (Figs. 3b, 6b, 9b and 11b) determined by thermal conductivities of the end plates. The temperature wall in the cells blocks further conduction of heat generated by other cells contingent on their location, and strongly influences the static and dynamic characteristics;

- The heat conductivity of the membrane varies during operations because of the continuous variation of water content and the consequent swelling phenomena, which results in an increase of electrical and thermal resistance.
- The latent heat of water produced at the catalysts by the reactions can be stored in the stack and requires a proper cooling strategy at a start-up when the cathode outlet gas does not sufficiently carry all the water vapor. In this case, the time necessary for a start-up is relatively short. Thus, the temperature difference between the central cells and the end cells is larger than the one with water removal during the vapor phase.
- Non-uniform temperature distribution through the stack can be minimized by properly coupling the coolant for the central cells with the end cells which can offset the temperature of the end cells.

5. Future work

We plan to add an accurate mass transport model to the current stack model to study the dynamic effects of fuels and reactants on the stack. The models will then be integrated into the exiting system model and implemented on a real-time system to optimize components of a fuel cell power system and design advanced controls. Further improvements are anticipated by taking into account the gas dynamics in the flow channel. At the same time, we plan to validate the models in close collaboration with industries and are looking for a partner to work with.

Acknowledgement

Yuyao Shan is grateful for the fellowship from the Department of Mechanical Engineering at Auburn University.

References

[1] R.M. Moore, K.H. Hauer, D. Friedman, J. Cunningham, P. Badrinarayanan, S. Ramaswamy, A. Eggert, J. Power Sources 141 (2005) 272–285.
[2] J.T. Pukrushpan, H. Peng, A.G. Stefanopoulou, J. Dyn. Syst. Meas. Control 126 (March (1)) (2004) 14–25.
[3] B.R. Sivertsen, N. Djilali, J. Power Sources 141 (2005) 65–78.
[4] U. Pasaogullari, C.Y. Wang, J. Electrochem. Soc. 152 (2) (2005) A380–A390.
[5] D. Natarajan, T.V. Nguyen, J. Power Sources 115 (2003) 66–80.
[6] J.C. Amphlett, R.F. Mann, B.A. Peppley, P.R. Roberge, A. Rodrigues, J. Power Sources 61 (1996) 183–188.
[7] S.D. Gurski, D.J. Nelson, et al. SAE 2003 World Congress & Exhibition, Detroit.
[8] E.A. Muller, A.G. Stefanopoulou, Proceedings of FUELCELL 2005 Third International Conference on Fuel Cell Science Engineering and Technology, ASME, 2005.
[9] M. Sundaresan, R.M. Moore, J. Power Sources 145 (2) (2005) 534–545.
[10] M. Wohr, K. Bolwin, W. Schnurnberger, M. Fischer, W. Neubrand, G. Eigenberger, Int. J. Hydrogen Energy 23 (3) (1998) 213–218.
[11] V. Peinecke, Ph.D. Thesis, University of Karlsruhe, Germany, 1994.
[12] M. Lampinen, M. Fomino, J. Electrochem. Soc. 140 (1993) 3537–3546.
[13] B. Wetton, K. Promislow, A. Caglar, Second International Conference on Fuel Cell Science, Engineering and Technology Fuel Cell 2004, 2004.
[14] P. Berg, K. Promislow, J. St-Pierre, J. Stumper, B. Wetton, J. Electrochem. Soc. 151 (2004) A341–A353.
[15] Y. Shan, S.Y. Choe, J. Power Sources 145 (2005) 30–39.
[16] M. Ceraolo, C. Miulli, A. Pozio, J. Power Sources 113 (2003) 131–144.
[17] H. Ju, H. Meng, C.Y. Wang, Int. J. Heat Mass Transfer 48 (2005) 1303–1315.
[18] S. Shimpalee, S. Dutta, Numer. Heat Transfer, Part A 38 (2000) 111–128.
[19] Y.M. Ferng, Y.C. Tzang, B.S. Pei, C.C. Sun, A. Su, Int. J. Hydrogen Energy 29 (2004) 381–391.
[20] J.H. Lee, T.R. Lalk, J. Power Sources 73 (1998) 229–241.
[21] J.P. Meyers, DOE Freeze Workshop 2005.
[22] Y. Wang, C.Y. Wang, Electrochimica 50 (2005) 1307–1315.
[23] A. Rowe, X. Li, J. Power Sources 102 (2001) 82–96.